

Unconventional magnetism in the spin-orbit driven Mott insulators $\text{Ba}_3M\text{Ir}_2\text{O}_9$ ($M=\text{Sc}, \text{Y}$)

Tusharkanti Dey,^{1,*} R. Kumar,¹ A.V. Mahajan,^{1,†} S. D. Kaushik,² and V. Siruguri²

¹*Department of Physics, Indian Institute of Technology Bombay, Powai, Mumbai 400076, India*

²*UGC-DAE Consortium for Scientific Research, Mumbai Centre, R-5 Shed, Bhabha Atomic Research Centre, Mumbai 400085, India*

Abstract

We have carried out detailed bulk and local probe studies on the hexagonal oxides $\text{Ba}_3M\text{Ir}_2\text{O}_9$ ($M=\text{Sc}, \text{Y}$) where Ir is expected to have a fractional oxidation state of +4.5. In the structure, Ir-Ir dimers are arranged in an edge shared triangular network parallel to the ab plane. Whereas only weak anomalies are evident in the susceptibility data, clearer anomalies are present in the heat capacity data; around 10K for $\text{Ba}_3\text{ScIr}_2\text{O}_9$ and at 4K for $\text{Ba}_3\text{YIr}_2\text{O}_9$. Our ^{45}Sc nuclear magnetic resonance (NMR) lineshape (first order quadrupole split) is symmetric at room temperature but becomes progressively asymmetric with decreasing temperatures indicating the presence of developing inequivalent Sc environments. This is suggestive of distortions in the structure which could arise from progressive tilt/rotation of the IrO_6 octahedra with a decrease in temperature T . The ^{45}Sc NMR spectral weight shifts near the reference frequency with decreasing T indicating the development of magnetic singlet regions. Around 10K, a significant change in the spectrum takes place with a large intensity appearing near the reference frequency but with the spectrum remaining multi-peak. It appears from our ^{45}Sc NMR data that in $\text{Ba}_3\text{ScIr}_2\text{O}_9$ significant disorder is still present below 10K. In the case of $\text{Ba}_3\text{YIr}_2\text{O}_9$, the ^{89}Y NMR spectral lines are asymmetric at high temperatures but become nearly symmetric (single magnetic environment) below $T \sim 70\text{K}$. Our ^{89}Y spectra and T_1 measurements confirm the onset of long range ordering (LRO) from a bulk of the sample at 4K in this compound. Our results suggest that $\text{Ba}_3\text{YIr}_2\text{O}_9$ might be structurally distorted at room temperature (via, for example, tilt/rotations of the IrO_6 octahedra) but becomes progressively a regular triangular lattice with decreasing T . The effective magnetic moments and magnetic entropy changes are strongly reduced in $\text{Ba}_3\text{YIr}_2\text{O}_9$ as compared to those expected for a $S = 1/2$ system. Similar effects have been found in other iridates which naturally have strong spin-orbit coupling (SOC).

PACS numbers: 75.47.Lx, 76.60.-k, 75.70.Tj, 75.40.Cx

I. INTRODUCTION

Recently, iridium ($5d$) based oxides have been the attraction of materials researchers due to their interesting quantum states [1]. In the case of $3d$ based oxides, a large onsite Coulomb interaction (U) and crystal field splitting are the driving interactions and a small spin-orbit coupling (SOC) is generally considered as a perturbation. The large U drives them to a Mott insulating state. In the case of iridates, U is expected to be much smaller because of the extended nature of the $5d$ -orbitals and one might expect the iridates to be metallic rather than magnetic. In contradiction to this naive expectation, many iridates like Sr_2IrO_4 [2, 3], $(\text{Na}/\text{Li})_2\text{IrO}_3$ [4–6], $\text{Na}_4\text{Ir}_3\text{O}_8$ [7, 8], and $\text{Ba}_3\text{IrTi}_2\text{O}_9$ [9] are found to be insulators showing exotic magnetic properties. In these iridates, SOC is believed to be comparable to U . The interplay of SOC and U makes these materials Mott insulators through a different mechanism and are often called spin-orbit driven Mott insulators. Kim *et al.* [2, 3] first reported such a spin-orbit driven Mott insulating state in Sr_2IrO_4 . Here a large SOC splits the t_{2g} orbitals of $\text{Ir}^{4+}(5d^5)$ into a half filled $J_{eff} = 1/2$ doublet and a completely filled $J_{eff} = 3/2$ quadruplet. Further, even a small U can

split the narrow $J_{eff} = 1/2$ band into lower and upper Hubbard bands and the material becomes a spin-orbit driven Mott insulator. Rapid theoretical [10–14] and experimental advances are being made in this area. All the materials mentioned above have $\text{Ir}^{4+}(5d^5)$ oxidation state. Materials with iridium oxidation state other than 4+ are not explored much but could be interesting.

We have been searching for new candidates to study this spin-orbit driven physics further. We found the triple perovskite $\text{Ba}_3M\text{Ir}_2\text{O}_9$ series to be rather interesting because a wide range of elements with a variety of oxidation states can be fitted as M . Several reports are available where M is an alkaline metal, a transition metal or a rare earth material. The nominal oxidation state of Ir can be 5.5+ (for $M=\text{Li}^+, \text{Na}^+$ [15]), 5+ (for $M=\text{Zn}^{2+}, \text{Mg}^{2+}, \text{Ca}^{2+}, \text{Cd}^{2+}$ [16]), 4.5+ (for $M=\text{Y}^{3+}, \text{Sc}^{3+}, \text{In}^{3+}, \text{Lu}^{3+}$ [16, 17]) and 4+ (for $M=\text{Ti}^{4+}, \text{Zr}^{4+}$ [16]). In all these compounds, Ir-Ir structural dimers are formed parallel to the crystallographic c -axis and these dimers are connected with each other to form an edge shared triangular lattice in the ab -plane. Novel properties are expected from this structural arrangement in addition to those driven by SOC.

The materials with a fractional oxidation state of Ir are even more interesting because the fractional oxidation state of Ir (accompanied by a unique crystallographic site) can lead them to a metallic state. Sakamoto *et al.* [16] reported results of magnetic susceptibility and heat capacity measurements on $\text{Ba}_3\text{Sc}^{3+}\text{Ir}_2^{4.5+}\text{O}_9$. An anomaly at 10K was seen in the heat capacity data (al-

*Present address: Leibniz-Institute for Solid State and Materials Research, IFW Dresden, 01171 Dresden, Germany

†Electronic address: mahajan@phy.iitb.ac.in

though it was not as sharp as normally seen for long-range ordering). The temperature derivative of the susceptibility also showed an anomaly at the same temperature. They suggested that the anomalies arose from the antiferromagnetic (AF) ordering of the spins. A Curie-Weiss (CW) fitting of the susceptibility data yielded a large AF Weiss temperature $\theta_{CW} = -570\text{K}$ and an effective magnetic moment $\mu_{eff} = 1.27\mu_B/\text{Ir}$. Such a large AF θ_{CW} and a much reduced magnetic ordering temperature indicates presence of frustration in the system. On the other hand, the Y-analog, $\text{Ba}_3\text{Y}^{3+}\text{Ir}_2^{4.5+}\text{O}_9$ [17] showed a sharper anomaly at 4K in the heat capacity data although no such feature was seen in the susceptibility data. A CW fitting of the susceptibility data in this case was not found to be satisfactory. A low moment found in both the cases was explained by formation of antiferromagnetic dimers [16, 17]. However a characteristic broad maximum followed by an exponential fall of susceptibility with decreasing temperature was not seen in either of the cases. These facts inspired us to take up the study of these two materials (*i.e.*, with $M=\text{Y, Sc}$) in detail. When reacted under high pressure, $\text{Ba}_3\text{YIr}_2\text{O}_9$ becomes cubic and the long-range ordering (LRO) disappears. We have earlier reported our results on the high pressure phase of $\text{Ba}_3\text{YIr}_2\text{O}_9$ and compared our results with the ambient pressure phase [18]. We have suggested that the high pressure phase is a spin-orbit driven gapless spin-liquid.

Nuclear magnetic resonance (NMR) is a very useful technique and widely used in strongly correlated electron systems to understand various physics issues like spin gap [19–22], magnetic ordering [23–26], superconductivity [27–29] etc. However in this newly developing field of SOC driven materials, to the best of our knowledge, very few [18, 30–32] NMR results have been reported. As iridium is a good absorber of neutrons, iridates are not easily probed by neutron diffraction/scattering. In these $\text{Ba}_3M\text{Ir}_2\text{O}_9$ ($M=\text{Sc, Y}$) materials, NMR could be a very useful local probe to throw light on their magnetism. In fact in the present case, while we found magnetic ordering from ^{89}Y NMR measurements in $\text{Ba}_3\text{YIr}_2\text{O}_9$, ordering could not be detected from neutron diffraction experiments. Also, as discussed earlier, an exponential fall of susceptibility (characteristic of antiferromagnetic dimer systems) was not seen in the case of these materials. Sometimes in bulk measurements the intrinsic susceptibility gets dominated by extrinsic effects. Using a local probe like NMR enables one to track the intrinsic susceptibility via the NMR shift measurement [33, 34]. Here in this paper, we report the results of our magnetization, heat capacity, and NMR measurements (^{45}Sc and ^{89}Y) on ambient pressure phases of $\text{Ba}_3M\text{Ir}_2\text{O}_9$ ($M=\text{Sc, Y}$). In addition to the bulk measurements, our NMR measurements confirm LRO at 4K for $\text{Ba}_3\text{YIr}_2\text{O}_9$. While the ^{89}Y NMR spectrum at high temperature seems typical of a powder pattern with axially symmetric shift anisotropy, the asymmetry decreases with decreasing temperature. One could also speculate that there is distribution of Y

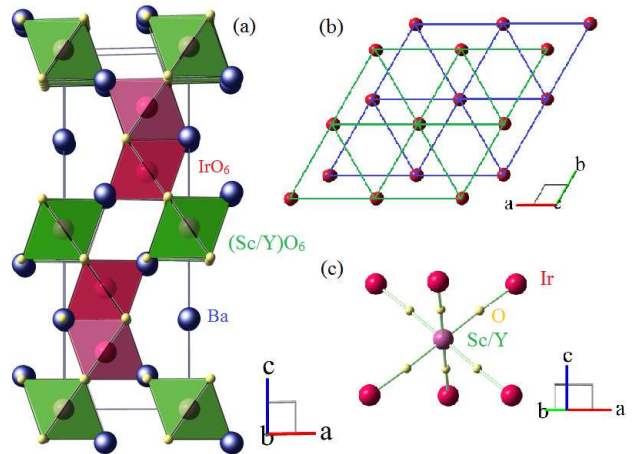


Figure 1: (a) The unit cell of the $\text{Ba}_3(\text{Y/Sc})\text{Ir}_2\text{O}_9$ system. (b) The edge shared triangular network in the ab plane formed by the Ir-Ir dimers is shown. (c) The Sc/Y environment is shown.

environments at room temperature which evolves into a single environment with a decrease in temperature, possibly changing from a distorted triangular lattice at high temperature to a near-perfect triangular lattice at lower temperatures with eventual ordering near 4K. On the other hand, in $\text{Ba}_3\text{ScIr}_2\text{O}_9$, no anomaly is seen in the magnetization data while only a miniscule difference is present in the zero field cooled (ZFC) and field cooled (FC) susceptibilities in a 100Oe field below about 8K. A weak and broad heat capacity anomaly is seen around this temperature. Our ^{45}Sc NMR measurements in $\text{Ba}_3\text{ScIr}_2\text{O}_9$ indicate that at room temperature, there is a single local environment for Sc suggesting a near-perfect triangular lattice. With decreasing temperature, the ^{45}Sc NMR line becomes asymmetric with increasing weight around the reference frequency. This could arise from progressive distortions in the structure in some regions (for instance, via tilt/rotation of the IrO_6 octahedra) leading to deviations from magnetic triangular lattice. The progressive increase of the spectral weight near the reference frequency is suggestive of a crossover to a singlet state. Finally, below about 10K, there is a significant change in the lineshape with a large peak near the reference frequency. In accord with this, the ^{45}Sc NMR spin-lattice relaxation rate $1/T_1$ corresponding to the zero-shifted line becomes small at low temperature, indicating the absence of magnetic fluctuations. The spectrum, however, remains multi-peak and suggests the presence of significant disorder.

II. EXPERIMENTAL DETAILS

Polycrystalline samples of $\text{Ba}_3M\text{Ir}_2\text{O}_9$ ($M=\text{Sc, Y}$) were prepared by solid state reaction method as detailed in Refs. [16] and [17]. We have used high purity BaCO_3 ,

Sc₂O₃/Y₂O₃ and Ir metal powder as starting materials. Sc₂O₃ and Y₂O₃ powders were pre-dried at 1000^oC overnight. Stoichiometric amount of the powders were mixed thoroughly, pressed into pellets and calcined at 900^oC for 12h. After calcination, the pellet was crushed into powder and again pelletized and fired at 1300^oC for 100h with intermediate grindings.

Powder x-ray diffraction (xrd) with Cu K_{α} radiation ($\lambda = 1.54182\text{\AA}$) and neutron diffraction ($\lambda = 1.48\text{\AA}$) measurements (for Ba₃YIr₂O₉) were carried out at room temperature for structural characterization. The magnetization M measurements were done in the temperature (T) range 2 – 400K and field (H) range 0 – 70kOe using a Quantum Design SQUID VSM. Heat capacity measurements were performed using the heat capacity attachment of a Quantum Design PPMS. The ⁴⁵Sc and ⁸⁹Y NMR measurements were done in a fixed magnetic field of 93.954kOe obtained inside a room-temperature bore Varian superconducting magnet. We have used a Tecmag pulse spectrometer for our measurements. For variable temperature measurements, an Oxford continuous flow cryostat was used with liquid nitrogen in the temperature range 80 – 300K and liquid helium in the temperature range 4 – 80K. The ⁴⁵Sc and ⁸⁹Y nuclear parameters are shown in Table I. Spectral lineshape was obtained by Fourier transform of the spin echo signal resulting from a $\pi/2 - \tau - \pi$ pulse sequence. Spin-lattice relaxation time was measured by the saturation recovery method. Spin-spin relaxation measurements were carried out using a standard $\pi/2 - t - \pi$ pulse sequence. Spin-spin relaxation time (T_2) was obtained by fitting the time dependence of spin-echo intensity $m(t)$ with

$$m(t) = m(0) \exp(-2t/T_2) \quad (1)$$

Since the bulk data for the title compounds have been reported earlier, we enumerate below our main conclusions concerning the xrd, magnetization and heat capacity measurements. To avoid repetition, only relevant figures are shown where the analysis is standard.

1. We were able to refine our xrd data for both the compounds corresponding to the space group P6₃/mmc. From our refinement, we found a small ($\sim 6\%$) site disorder between Sc³⁺ ions at the $2a$ site and Ir^{4.5+} ions at the $4f$ site for Ba₃ScIr₂O₉ which is similar to the site disorder (5.5%) found by Sakamoto *et al.* [16]. Figs. 1(a) and (b) illustrate the main feature of the structure, namely, Ir-Ir dimers forming edge shared triangles. The Y/Sc environment is demonstrated in Fig. 1(c).
2. For both the compounds, the susceptibility has a Curie-Weiss (CW) nature, $\chi = \chi_0 + C/(T - \theta_{CW})$. Also, while the Sc-compound shows no anomaly in $\chi(T)$, a weak anomaly at about 4K was observed in the Y-compound (see Fig. 9). Note however that for the Sc-compound the susceptibility has very little T -dependence down to nearly 50K (see Fig. 4)

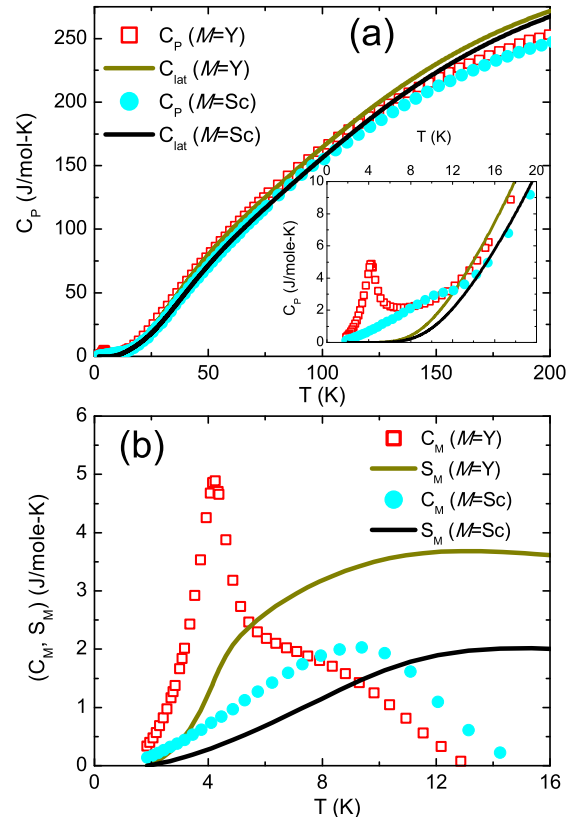


Figure 2: (a) The heat capacities (C_P) of Ba₃M Ir₂O₉ ($M=Sc, Y$) samples measured in zero field and their fitting with the Debye model (solid lines) are shown. Inset: The low-temperature part of the C_P data are shown along with the extrapolated Debye fit curve. (b) The magnetic heat capacity C_M (per mole formula unit) obtained by subtracting the lattice part from C_P is shown. Typical error bars are indicated for a few points. The corresponding entropy changes (ΔS_M) for both the samples are also shown.

and hence the θ_{CW} and C values obtained for this compound should be taken with caution. In any case, the effective moments ($\mu_{eff} \simeq \sqrt{8C}$) for the Sc and the Y-compounds were $1.4\mu_B$ and $0.3\mu_B$ which are much smaller than that corresponding to (say) $S = 1/2$. In other iridate systems as well, effective paramagnetic moments much smaller than the pure spin value have been observed [9, 35]. This is believed to happen due to partial cancellation of the spin and orbital part coupled via SOC [14]. The θ_{CW} values obtained from the fit are -588 K and ~ 0 K for the Sc and Y-compounds, respectively.

3. The measured heat capacity $C_P(T)$ (which includes the lattice contribution) shows a sharp anomaly at

Table I: Nuclear parameters of ^{45}Sc and ^{89}Y

Nucleus	Spin (I)	Gyromagnetic ratio $\gamma/2\pi$	Natural abundance
^{45}Sc	7/2	10.343 MHz/T	100%
^{89}Y	1/2	2.0859 MHz/T	100%

about 4K for the Y-compound but only a weak broad hump around 10K for the Sc-compound (Fig. 2(a)). This suggests a transition to long-range order in the former compound. A good fit to the high- T data was obtained using a combination of one Debye term and 3 Einstein terms with coefficients in the ratio 1:1:5:8. The magnetic heat capacity $C_M(T)$ was obtained upon subtracting this lattice contribution (Fig. 2(b)). Subsequently, integrating $C_M(T)$ gave the entropy change (ΔS_M) associated with the magnetic ordering for both the systems. The values of ΔS_M obtained from our analysis are 2J/mole K and 3.6J/mole K for the Sc-compound and the Y-compound, respectively. These are similar to those obtained in Ref.[16, 17]. The expected value of the entropy change $R\ln(2S + 1)$ is 5.76J/mol-K for $S = 1/2$, 9.13J/mol-K for $S = 1$ and 11.52J/mol-K for $S = 3/2$. A decrease in the entropy change has also been observed in other iridate systems such as Sr_2IrO_4 [36] and Na_2IrO_3 [37]. Finally, although the systems are very similar, the entropy change for $\text{Ba}_3\text{ScIr}_2\text{O}_9$ is only $\sim 50\%$ of the entropy change in $\text{Ba}_3\text{YIr}_2\text{O}_9$.

III. NMR RESULTS AND DISCUSSION

After some basic characterization, we have performed ^{45}Sc NMR and ^{89}Y NMR studies on $\text{Ba}_3\text{ScIr}_2\text{O}_9$ and $\text{Ba}_3\text{YIr}_2\text{O}_9$ in the T range 4 – 300K which is discussed below. The different parameters for ^{45}Sc and ^{89}Y nuclei are shown in Table I.

A. ^{45}Sc NMR in $\text{Ba}_3\text{ScIr}_2\text{O}_9$

First, let us consider the spectrum at 300K. Since ^{45}Sc has nuclear spin $I = 7/2$, one expects the spectrum to be a quadrupolar powder pattern. However, the spectrum at room temperature (inset of Fig. 3(a)) has a symmetric central line (shifted negatively, i.e., towards lower frequencies, with respect to the reference frequency) with full width at half maxima (FWHM) about 10kHz while the satellite peaks have a much reduced intensity. It appears that the electric field gradient is not very significant as ^{45}Sc is in an octahedral environment which is not strongly distorted. The observed spectrum at 300K is compared with a combination of a quadrupole split powder pattern (spectrum A) with $\nu_Q = 230\text{kHz}$ and another one with only a coincident central line (spectrum

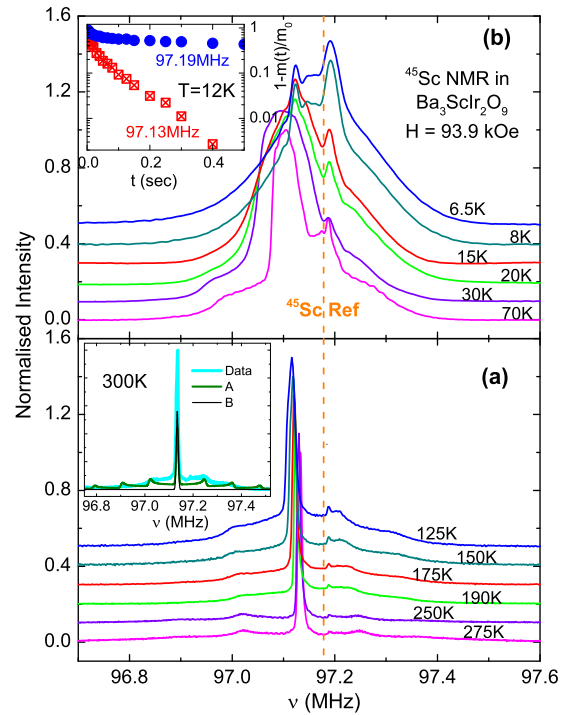


Figure 3: The ^{45}Sc NMR spectra of $\text{Ba}_3\text{ScIr}_2\text{O}_9$ at different temperatures are shown. The lower panel (a) shows the higher temperature ($T \geq 125\text{K}$) spectra and the upper panel (b) shows lower temperature ($T \leq 70\text{K}$) ones. The individual spectrum are shifted vertically by 0.1 from the previous one to have clarity. The dashed lines indicate the ^{45}Sc reference frequency. Lower inset: Spectrum at 300K is shown as thick blue line. The spectrum could be simulated by a combination of a quadrupole split powder pattern (A) and a single line (B). The amplitude ratio of A and B is 0.45 : 0.55 (see text). Upper inset: Longitudinal nuclear magnetization recovery curves measured at different transmitter frequencies at 12K.

B) with $\nu_Q = 0$ (see inset of Fig. 3(a)). Similar analysis is also done for ^{45}Sc NMR spectra in $\text{Ba}_3\text{Cu}_3\text{Sc}_4\text{O}_{12}$ [38]. The mismatch in the intensity in the frequency region between the central line and the satellite anomaly might imply that there is a distribution of environments for ^{45}Sc nuclei, ranging from a nearly perfect octahedral symmetry to those with lattice distortions.

We next look at the evolution of the spectrum as a function of temperature which is shown in Fig. 3. As is clear, with decreasing temperature, the peak moves to lower frequencies and the spectrum broadens. Since the peak shifts negatively as temperature is decreased while $\chi(T)$ increases in a CW manner, it appears that the po-

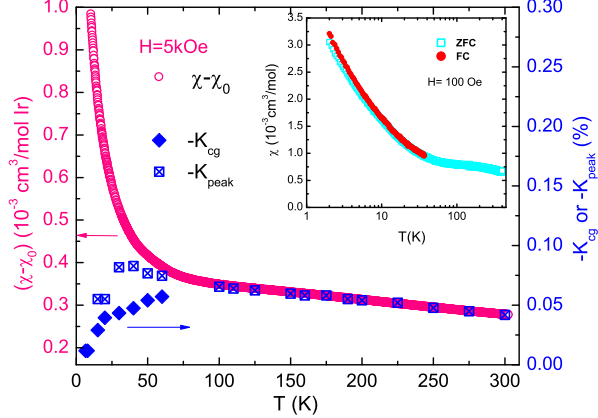


Figure 4: The bulk susceptibility ($\chi - \chi_0$) of $\text{Ba}_3\text{ScIr}_2\text{O}_9$ is shown as function of temperature on the left axis. The temperature variation of ^{45}Sc NMR shift obtained from center-of-gravity ($-K_{cg}$) and also from the peak position ($-K_{peak}$) (at low temperature) are shown on the right axis. Inset: The ZFC and FC susceptibilities of $\text{Ba}_3\text{ScIr}_2\text{O}_9$ are shown as a function of temperature in a semi-log scale.

sition of the central line actually tracks $\chi(T)$ with a negative hyperfine coupling. This is illustrated in Fig. 4 where we have plotted the bulk susceptibility ($\chi - \chi_0$) as a function of temperature on the left axis while $-K_{cg}$ or $-K_{peak}$ are plotted on the right axis. Here the shift is expressed in percent as, for instance, $K_{peak} = \frac{\nu_{peak} - \nu_0}{\nu_0} \times 100$ where ν_{peak} is the peak frequency and ν_0 is the reference frequency. For temperatures above 100K, the shift K_{peak} is obtained from the maximum of the central line. At lower temperatures, another peak begins to develop near the reference frequency and so we have plotted both $-K_{peak}$ and $-K_{cg}$, the latter obtained from the center of gravity of the spectrum. It is seen that both $-K_{peak}$ and $-K_{cg}$ decrease towards zero at low temperature, in contrast to the bulk susceptibility. The upturn seen in $\chi(T)$ must then be of extrinsic origin. By subtracting the intrinsic susceptibility (inferred from the NMR shift) from the measured one, we obtain the Curie behaviour due to extrinsic paramagnetic impurities which are estimated to be about 3% of $S = 1/2$ entities. Note that the peak in the ^{45}Sc spectra near the reference frequency can not be from some impurity phase since its relative intensity increases at low temperature [39]. These observations suggest that the system progressively goes to a nonmagnetic state at low temperatures. From the plot of $-K_{cg}$ as a function of $(\chi - \chi_0)$ (not shown), which is linear in the temperature range 75 – 300K, we have calculated $A_{hf} = -2.994\text{kOe}/\mu_B$. Finally, note that there is an abrupt change in the lineshape around 10K, the temperature at which there is a heat capacity anomaly. Whereas the strange lineshape below 10K could be due to some peculiar spin order, sharp peaks at around 97.13 MHz

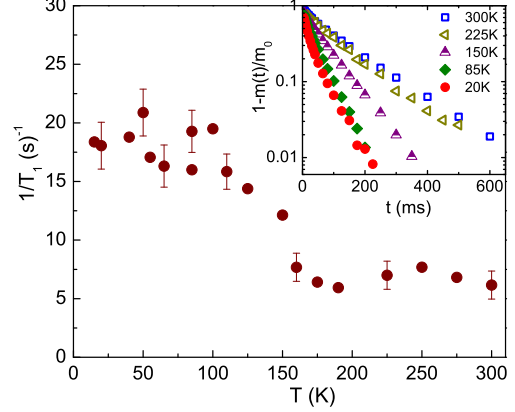


Figure 5: The ^{45}Sc spin lattice relaxation rates ($1/T_1$) of $\text{Ba}_3\text{ScIr}_2\text{O}_9$ are shown as a function of temperature. Inset: The longitudinal nuclear magnetization recovery data for $\text{Ba}_3\text{ScIr}_2\text{O}_9$ are shown at a few temperatures in a semi-log scale. The transmitter frequency was fixed at that of the main peak, around 97.13MHz.

and 97.19 MHz emerge already above 20K and do not shift with temperature. The root cause of this strange lineshape is not unambiguously clear at the moment.

Since it is clear from the discussion so far that the ^{45}Sc nuclei track the magnetic susceptibilities of the iridium ions, magnetic fluctuations associated with Ir should impact the ^{45}Sc NMR spin-lattice relaxation rate ($1/T_1$) and its variation with temperature. Most of our $1/T_1$ data were taken with the transmitter frequency coincident with that of the main peak, i.e., around 97.13MHz. A few representative longitudinal nuclear magnetization recovery data are shown in the inset of Fig. 5. All the recovery curves have an initial fast component followed by a single exponential decay at higher delays. Since ^{45}Sc is a quadrupolar nucleus, in case the central line and the satellites are not fully irradiated, the recovery of the longitudinal nuclear magnetization is not expected to be single exponential [43, 44]. In the present case, due to the relatively small ν_Q , we are in a situation of nearly full saturation of the satellites. In any case, by measuring the slope of the long time recovery, we can extract $1/T_1$ which is what we have done. Temperature variation of $1/T_1$ is shown in Fig. 5. It can be seen that from room temperature down to $\sim 175\text{K}$, $1/T_1$ is almost constant as would be the case in the paramagnetic regime. Below 175K it increases with decreasing temperature but again becomes almost constant below about 100K. The increase suggests the building up of magnetic correlations but there is an inability to order due possibly to the geometric frustration. The leveling off near 100K is again commensurate with the growth of non-magnetic regions as seen from the spectra. Also, a representative T_1 measurement taken near the reference frequency (97.19MHz) indicates that the corresponding

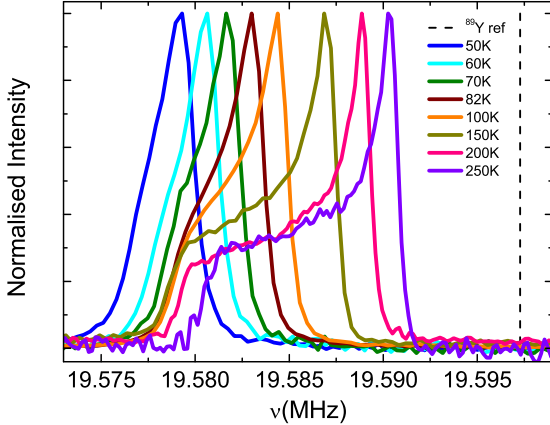


Figure 6: The ^{89}Y NMR spectral lines in the temperature range 50 – 250K. The ^{89}Y reference position is shown as dashed line.

relaxation rate is much smaller than that at the main peak (see inset of Fig. 3(b)). This is further indication that the peak near the reference frequency arises from nonmagnetic regions. The absence of any divergence of $1/T_1$ with temperature down to 4K means that a large part of the sample remains disordered in this temperature range. These data are somewhat reminiscent of the $\text{LiZn}_2\text{Mo}_3\text{O}_8$ system where the data (a broad crossover in the susceptibility, a hump in the specific heat, and no ordered moments [42]) suggest a gradual “gapping out” rather than a phase transition. There, a physical distortion of the triangular lattice giving rise to a decoupling of the honeycomb lattice from the central spins has been suggested [40, 41]. Whether a similar outcome (gradual gapping out in some regions of the sample) is evident in our Sc-system is not clear though if that were to be the case, we do not seem to sense the Curie contribution of the central spins in the evolution of the ^{45}Sc NMR lineshape with temperature.

With the above background, we next focus on the isostructural compound $\text{Ba}_3\text{YIr}_2\text{O}_9$. In this system, the aspects that are different from the Sc-system and might be to our advantage are (i) ^{89}Y has nuclear spin $I = 1/2$ hence there will be no quadrupolar effect and (ii) the near-absence of a site disorder between Y and Ir.

B. ^{89}Y NMR in $\text{Ba}_3\text{YIr}_2\text{O}_9$

Evolution of the ^{89}Y spectral shape, shift and relaxation rates in $\text{Ba}_3\text{YIr}_2\text{O}_9$ as a function of temperature are discussed in the following.

The ^{89}Y spectra in $\text{Ba}_3\text{YIr}_2\text{O}_9$ are narrow ($\sim 8 - 10\text{kHz}$) except for the one at 4K. As shown in Fig. 6, the spectral line at 250K is asymmetric with a sharp peak on the right side and a shoulder on the left. The spec-

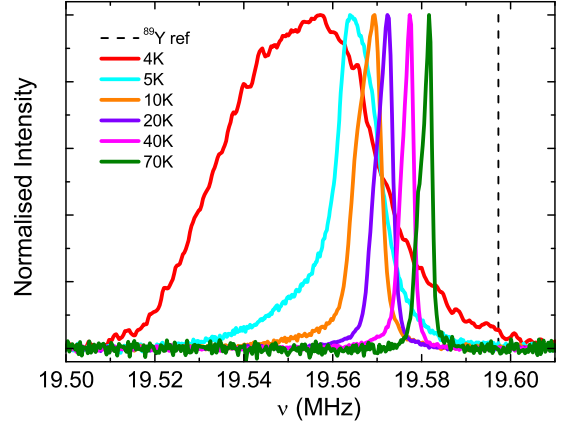


Figure 7: The temperature evolution of ^{89}Y NMR spectra in the range 4 – 70K for $\text{Ba}_3\text{YIr}_2\text{O}_9$ is shown. The sudden change in the spectrum at 4K is probably due to long range ordering. The ^{89}Y reference is also shown as a dashed line.

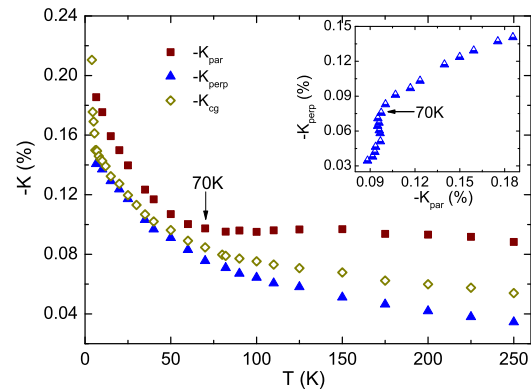


Figure 8: The temperature evolution of different shift parameters for $\text{Ba}_3\text{YIr}_2\text{O}_9$. Inset: $-K_{perp}$ is shown as a function of $-K_{par}$.

trum at 250K is on the left side of the reference line and therefore has a negative shift. Such a lineshape looks typical of a powder pattern with an axially symmetric Knight shift tensor. However, the temperature dependence of the anisotropic components $-K_{par}$ (contribution from $\theta = 0$, i.e., field along the axis) and $-K_{perp}$ (contribution from $\theta = 90^\circ$, i.e., field perpendicular to the axis), as shown in Fig. 8, is unusual. Although the average shift **increases** in a Curie-like manner tracking the bulk susceptibility, $-K_{par}$ is nearly unchanged at high-temperature while it tracks $-K_{perp}$ below 70K or so. This is also illustrated in $-K_{perp}$ vs. $-K_{par}$ plot (inset of Fig. 8) which is not linear. This would imply that either the susceptibility anisotropy or the hyperfine coupling anisotropy changes with temperature. Another

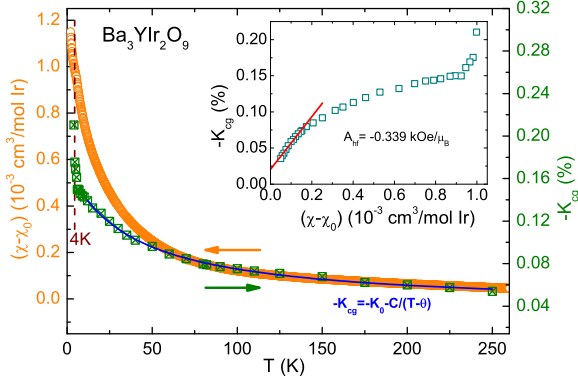


Figure 9: The bulk susceptibility ($\chi - \chi_0$) of $\text{Ba}_3\text{YIr}_2\text{O}_9$ (open circles) is shown as function of temperature on the left axis. The shift $-K_{cg}$ (green open squares) and its fit with the Curie-Weiss formula (blue solid line) are shown on the right axis as a function of T . The ordering temperature 4K is marked with a dashed line. Inset: $-K_{cg}$ is plotted against $(\chi - \chi_0)$ with temperature as the implicit parameter. The red solid line is a linear fit.

possibility is that the anisotropy of the lineshape arises from a distribution of magnetic environments for the ^{89}Y nuclei. The observed variation with temperature would then further imply that the local environments become more homogeneous with a decrease in temperature. One could then speculate that the distribution of magnetic environments comes from a distortion of the triangular lattice by rotations and tilts of the IrO_6 octahedra. One could then further speculate that distortions heal at lower temperatures and the lattice becomes more perfectly triangular and the system can then order (seen from the sudden increase in linewidth below about 4K). It is anyhow unusual for the anisotropy of the lineshape to decrease with temperature. In any case, this is in complete contrast to $\text{Ba}_3\text{ScIr}_2\text{O}_9$ where a symmetric lineshape at room temperature evolves to an asymmetric one at lower temperatures. It should be mentioned that in the case of Ba_2YMoO_6 also ^{89}Y spectral lineshape was observed to be asymmetric at high temperatures although there is a single Y site [31].

Since the spectral line is asymmetric at higher temperatures, we have calculated the shift taking the center-of-gravity (K_{cg}) of each spectrum. The temperature dependence of the shift ($-K_{cg}$) is shown in Fig. 9. The jump in the shift near 4K is most likely due to the magnetic ordering. We have fitted our shift data with the Curie-Weiss formula $-K_{cg} = -K_0 - C/(T - \theta)$ in the temperature range 10 – 250K. It is nicely fitted with the formula and we obtained $-K_0 = 0.0387\%$ and $\theta \sim -37\text{K}$, which means the interaction is antiferromagnetic in nature. With an ordering temperature of 4K, we get a frustration ratio $f = 37/4 > 9$ where the frustration comes from the edge-shared triangular structure.

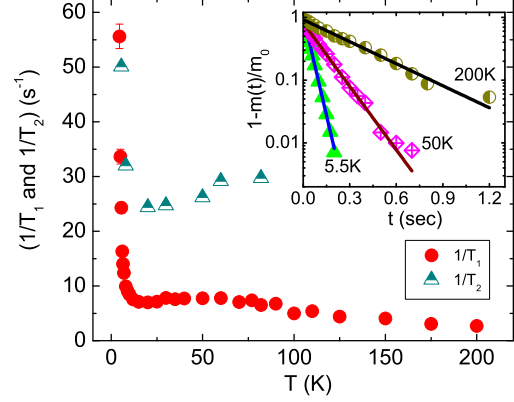


Figure 10: The spin-lattice relaxation rate ($1/T_1$) and spin-spin relaxation rates ($1/T_2$) are shown as a function of temperature. Inset: The longitudinal nuclear magnetization recovery curves at a few temperatures are shown along with their fits (solid line).

Next we have estimated the hyperfine coupling constant as follows. In the inset of Fig. 9, shift ($-K_{cg}$) is plotted as a function of $(\chi - \chi_0)$ which is linear above $\sim 60\text{K}$. From the slope of the line, we get the hyperfine coupling $A_{\text{hf}} = -0.339\text{kOe}/\mu_{\text{B}}$. The actual slope has been divided by 6 as ^{89}Y is hyperfine coupled to 6 Ir. The y -intercept of the line gives $-K_0 = -K_{\text{chem}} = 0.021\% = 210\text{ppm}$. It should be noted that for the cubic phase sample [18] of $\text{Ba}_3\text{YIr}_2\text{O}_9$, the shift is temperature independent and has $-K_0 = -K_{\text{chem}} = 0.064\% = 640\text{ppm}$. The deviation from linearity of the $K - \chi$ data (below about 60K) suggests a low temperature extrinsic Curie term in $\chi(T)$.

In contrast to the Sc-sample, the linewidth is small here and we find a single exponential behavior for the recovery of the longitudinal nuclear magnetization at all temperatures. A few representative recovery curves are shown in the inset of Fig. 10 with their fits. The spin lattice relaxation rate ($1/T_1$) is shown as a function of temperature in Fig. 10. At 200K, $1/T_1$ is small but slowly increases as temperature is decreased. This suggests building up of short range interactions between the spins. Once again, there is a change in the $1/T_1$ behavior around 70K precisely where the lineshape becomes symmetric and we have suggested that this reflects the “healing” of distortions at low temperatures. Below about 70K, $1/T_1$ becomes almost temperature independent down to 15K and increases below that. The divergence in $1/T_1$ at 4K is due to the critical slowing down of the spin fluctuations on approach to long-range ordering. The temperature variation of spin-spin relaxation rate ($1/T_2$) is plotted in Fig. 10 along with $1/T_1$. At higher temperatures $1/T_2$ is much larger (as might be expected) than $1/T_1$ but near 4K they become nearly equal which is another signature of long-range ordering.

IV. CONCLUSIONS

Both the systems studied here $Ba_3M\text{Ir}_2\text{O}_9$ ($M=\text{Sc}, \text{Y}$) show interesting properties. One might have expected them to be metallic because of the extended nature of the Ir $5d$ orbitals and the fractional valence of Ir. But in reality the samples are insulating and at least one of them ($Ba_3\text{YIr}_2\text{O}_9$) orders magnetically. In the case of $Ba_3\text{ScIr}_2\text{O}_9$, our local probe (NMR) data provide evidence that the sample is magnetically homogeneous at high temperatures, then the ^{45}Sc nuclei have distinct magnetic environments at intermediate temperatures and finally a large fraction of the system goes to a singlet state at low temperatures. The associated entropy change for $Ba_3\text{ScIr}_2\text{O}_9$ is almost 50% of that found in $Ba_3\text{YIr}_2\text{O}_9$ and much smaller than the theoretically expected value. The data on the Sc-system suggest a gradual “gapping out” as temperature is decreased though there is evidence of an abrupt change as well in the NMR lineshape around 10K. Whether there is any structural-distortion-assisted break-up of the triangular lattice into singlet entities is something that remains to be proven. From our NMR results we can say that the system is certainly interesting for further study, say, using muon spin rotation (μSR) as a local probe of magnetism. On the

other hand, in the case of $Ba_3\text{YIr}_2\text{O}_9$ the ^{89}Y lineshape is asymmetric at room temperature and progressively becomes more symmetric at lower temperatures. This could be due to a change, with temperature, of the anisotropy of the hyperfine couplings or due to a change in the distribution of magnetic environments. We feel that it is likely related to some subtle change in structural details (such as rotation/tilt of IrO_6 octahedra) with temperature which impacts the magnetism. The system orders magnetically at 4K. Nevertheless, a small Curie constant $C = 0.0125 \text{ cm}^3\text{K/mol-Ir}$ (30 times smaller than the $S = 1/2$ value) and a small entropy change is found in our measurements. These unusual features seem to be driven by the frustration due to the triangular network of Ir-Ir dimers in addition to a strong SOC present in the iridates.

V. ACKNOWLEDGEMENTS

We acknowledge the financial support from Indo-Swiss Joint Research Program, Department of Science and Technology, India. We thank H. M. Ronnow and I. Dasgupta for useful discussions.

-
- [1] For a review, see *Frontiers of 4d- and 5d- transition metal oxides*, edited by G. Cao and L. DeLong, World Scientific (2013)
 - [2] B. J. Kim, H. Jin, S. J. Moon, J.-Y. Kim, B.-G. Park, C. S. Leem, Jaeyun Yu, T.W. Noh, C. Kim, S.-J. Oh, J.-H. Park, V. Durairaj, G. Cao, and E. Rotenberg, *Phys. Rev. Lett.* **101**, 076402 (2008)
 - [3] B. J. Kim, H. Ohsumi, T. Komesu, S. Sakai, T. Morita, H. Takagi, and T. Arima, *Science* **323**, 1329 (2009)
 - [4] G. Cao, T. F. Qi, L. Li, J. Terzic, V. S. Cao, S. J. Yuan, M. Tovar, G. Murthy, and R. K. Kaul, *Phys. Rev. B* **88**, 220414(R) (2013)
 - [5] H. Gretarsson, J. P. Clancy, X. Liu, J. P. Hill, E. Bozin, Y. Singh, S. Manni, P. Gegenwart, J. Kim, A. H. Said, D. Casa, T. Gog, M. H. Upton, H.-S. Kim, J. Yu, V. M. Katukuri, L. Hozoi, J. van den Brink, and Y.-J. Kim, *Phys. Rev. Lett.* **110**, 076402 (2013)
 - [6] S. Manni, S. Choi, I. I. Mazin, R. Coldea, M. Altmeyer, H.O. Jeschke, R. Valenti, P. Gegenwart, arXiv:1312.0815v1 (unpublished)
 - [7] Y. Okamoto, M. Nohara, H. Aruga-Katori, and H. Takagi, *Phys. Rev. Lett.* **99**, 137207 (2007)
 - [8] Y. Singh, Y. Tokiwa, J. Dong, P. Gegenwart, *Phys. Rev. B* **88**, 220413(R) (2013)
 - [9] T. Dey, A. V. Mahajan, P. Khuntia, M. Baenitz, B. Koteswararao, and F. C. Chou, *Phys. Rev. B (R)* **86**, 140405 (2012)
 - [10] K.-Y. Yang, Y.-M. Lu, and Y. Ran, *Phys. Rev. B* **84**, 075129 (2011)
 - [11] G. Khaliullin, *Phys. Rev. Lett.* **111**, 197201 (2013)
 - [12] J. Chaloupka, G. Jackeli, and G. Khaliullin, *Phys. Rev. Lett.* **105**, 027204 (2010)
 - [13] F. Wang and T. Senthil, *Phys. Rev. Lett.* **106**, 136402 (2011)
 - [14] G. Chen, R. Pereira, and L. Balents, *Phys. Rev. B* **82**, 174440 (2010)
 - [15] S.-J. Kim, M. D. Smith, J. Darriet, and H.-C. zur Loye, *J. Solid State Chem.* **177**, 1493 (2004)
 - [16] T. Sakamoto, Y. Doi, and Y. Hinatsu, *J. Solid State Chem.* **179**, 2595 (2006)
 - [17] Y. Doi and Y. Hinatsu, *J. Phys.: Condens. Matter* **16**, 2849 (2004)
 - [18] T. Dey, A.V. Mahajan, R. Kumar, B. Koteswararao, F. C. Chou, A. A. Omrani, and H. M. Ronnow, *Phys. Rev. B* **88**, 134425 (2013)
 - [19] J. Bobroff, N. Laflorencie, L. K. Alexander, A. V. Mahajan, B. Koteswararao, and P. Mendels, *Phys. Rev. Lett.* **103**, 047201 (2009)
 - [20] H. Iwase, M. Isobe, Y. Ueda and H. Yasuoka, *J. Phys. Soc. Jpn.* **65**, 2397 (1996)
 - [21] M.-H. Julien, P. Carretta, M. Horvatić, C. Berthier, Y. Berthier, P. Ségransan, A. Carrington, and D. Colson, *Phys. Rev. Lett.* **76**, 4238 (1996)
 - [22] C. S. Lue, S. C. Chen, C. N. Kuo, and F. C. Chou, *Phys. Rev. B* **80**, 092407 (2009)
 - [23] L. K. Alexander, N. Büttgen, R. Nath, A. V. Mahajan, and A. Loidl, *Phys. Rev. B* **76**, 064429 (2007)
 - [24] A. A. Gippius, E. N. Morozova, A. S. Moskvin, A. V. Zalessky, A. A. Bush, M. Baenitz, H. Rosner, and S.-L. Drechsler, *Phys. Rev. B* **70**, 020406(R) (2004)
 - [25] S. Ohsugi, K. Magishi, S. Matsumoto, Y. Kitaoka, T. Nagata, and J. Akimitsu, *Phys. Rev. Lett.* **82**, 4715 (1999)
 - [26] R. Nath, A. V. Mahajan, N. Büttgen, C. Kegler, A. Loidl, and J. Bobroff, *Phys. Rev. B* **71**, 174436 (2005)

- [27] J. Bobroff, H. Alloul, S. Ouazi, P. Mendels, A. Mahajan, N. Blanchard, G. Collin, V. Guillen, and J.-F. Marucco, *Phys. Rev. Lett.* **89**, 157002 (2002)
- [28] Y. Nakai, T. Iye, S. Kitagawa, K. Ishida, H. Ikeda, S. Kasahara, H. Shishido, T. Shibauchi, Y. Matsuda, and T. Terashima, *Phys. Rev. Lett.* **105**, 107003 (2010)
- [29] K. Ishida, Y. Nakai, and H. Hosono, *J. Phys. Soc. Japan* **78**, 062001 (2009) and references therein
- [30] See <http://online.itp.ucsb.edu/online/motterials07/takagi>
- [31] T. Aharen, J. E. Greedan, C. A. Bridges, A. A. Aczel, J. Rodriguez, G. MacDougall, G. M. Luke, T. Imai, V. K. Michaelis, S. Kroeker, H. Zhou, C. R. Wiebe, and L. M. D. Cranswick, *Phys. Rev. B* **81**, 224409 (2010)
- [32] T. Aharen, J. E. Greedan, F. Ning, T. Imai, V. Michaelis, S. Kroeker, H. Zhou, C. R. Wiebe, and L. M.D. Cranswick, *Phys. Rev. B* **80**, 134423 (2009)
- [33] J. A. Quilliam, F. Bert, E. Kermarrec, C. Payen, C. Guillot-Deudon, P. Bonville, C. Baines, H. Luetkens, and P. Mendels, *Phys. Rev. Lett.* **109**, 117203 (2012)
- [34] T. Imai, E. A. Nytko, B. M. Bartlett, M. P. Shores, and D. G. Nocera, *Phys. Rev. Lett.* **100**, 077203 (2008)
- [35] G. Cao, J. Bolivar, S. McCall, J. E. Crow, and R. P. Guertin, *Phys. Rev. B* **57**, R11039 (1998)
- [36] S. Chikara, O. Korneta, W. P. Crummett, L. E. DeLong, P. Schlottmann, and G. Cao, *Phys. Rev. B* **80**, 140407(R) (2009)
- [37] Y. Singh and P. Gegenwart, *Phys. Rev. B* **82**, 064412 (2010)
- [38] B. Koteswararao, A.V. Mahajan, F. Bert, P. Mendels, J. Chakraborty, V. Singh, I. Dasgupta, S. Rayaprol, V. Siruguri, A. Hoser and S. D. Kaushik, *J. Phys.: Condens. Matter* **24**, 236001 (2012)
- [39] It is true that due to a possible contrast in the spin-spin relaxation times T_2 for the two peaks at low temperature (a much longer T_2 for the unshifted peak compared to the main peak), one can artificially enhance the intensity of the peak near the reference position. We have therefore taken care of this and kept the time delay between the echo producing *rf* pulses to be several times shorter than the shortest T_2 . Further, the repetition time of the pulse sequence was several times the longest T_1 . The Sc/Ir site mixing might also contribute to the unshifted peak though the intensity should not change with temperature. We also confirmed that the total integrated spectral intensity times the temperature is nearly constant below, say, 50K.
- [40] R. Flint and P. A. Lee, *Phys. Rev. Lett.* **111**, 217201 (2013)
- [41] M. Mourigal, W. T. Fuhrman, J. P. Sheckelton, A. Wartelle, J. A. Rodriguez-Rivera, D. L. Abernathy, T. M. McQueen, and C. L. Broholm, *Phys. Rev. Lett.* **112**, 027202 (2014)
- [42] J. P. Sheckelton, J. R. Neilson, D. G. Soltan, and T. M. McQueen, *Nat. Mater.* **11**, 493 (2012)
- [43] In case, one irradiates only the central line and the duration of the saturating sequence is much less than T_1 , the recovery law is given by
- $$1-m(t)/m_0 = A [0.011905 \exp(-t/T_1)+0.068182 \exp(-6t/T_1)+0.20605 \exp(-6t/T_1)]$$
- In case, the duration of the saturating comb is much greater than T_1 (with only the central line getting saturated), then the recovery law is
- $$1-m(t)/m_0 = A [0.190476 \exp(-t/T_1)+0.181819 \exp(-6t/T_1)+0.21978 \exp(-6t/T_1)]$$
- However, if the central line is fully saturated and the satellites are also partly saturated, the coefficient of the e^{-t/T_1} term will be greater than given above and will approach one for full saturation. In case of a small weight for the e^{-t/T_1} term, recovery would have attained a linear behaviour (on a log-linear scale) only at very long times, in contrast to our data.
- [44] A. Suter, M. Mali, J. Roos, and D. Brinkmann, *J. Phys.: Condens. Matter* **10**, 5977 (1998)